Computational and experimental study of the synchronization strategies of two pulsing jet fluidic oscillators

Shiqi Wang, Ahmad Batikh, Lucien Baldas, Azeddine Kourta, Nicolas Mazellier, Stéphane Colin, Stéphane Orieux

Sensors & Actuators: A. Physical 369 (2024) 115165

Contents lists available at ScienceDirect

Sensors and Actuators: A. Physical

journal homepage: www.journals.elsevier.com/sensors-and-actuators-a-physical

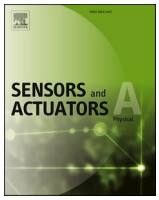

Computational and experimental study of the synchronization strategies of two pulsing jet fluidic oscillators

Shiqi Wang [a,b], Ahmad Batikh [a,c,*], Lucien Baldas [a], Azeddine Kourta [d], Nicolas Mazellier [d], Stéphane Colin [a], Stéphane Orieux [a]

[a] Institut Clément Ader (ICA), Université de Toulouse, CNRS, INSA, ISAE-SUPAERO, Mines-Albi, UPS, Toulouse, France
[b] Aero-Engine Academy of China, Aero-Engine Corporation of China, Beijing 101304, China
[c] Icam School of Engineering, Toulouse campus, 75 Avenue de Grande Bretagne, CS 97615, 31076 Toulouse Cedex 3, France
[d] Université d'Orléans, INSA-CVL, PRISME EA 4229, Orléans F45072, France

ARTICLE INFO

Keywords:
Bi-stable fluidic oscillator
Active flow control actuator
Synchronization
Oscillation dynamics
CFD

ABSTRACT

Fluidic oscillators are interesting actuators for flow control purposes as they produce unsteady jets without any moving part. Flow separation control in a large scale, for instance on a wing, needs an array of such actuators, whose efficiency can be improved if the pulsed jets are synchronized. In this paper, two synchronization configurations based on interconnections of the feedback loops have been applied successfully to two bi-stable fluidic oscillators. The first configuration permits to obtain jets pulsating at a similar frequency as the jets produced by the oscillators working separately. The second configuration, which differs by the interconnection pattern, leads to a much lower frequency. Two different phase lags between the jets produced by the two oscillators have also been identified, depending on the interconnection pattern. These experimental results have been completed by a numerical study of the internal flow patterns of the two oscillators for an in-depth analysis of the physical mechanisms controlling the oscillation dynamics. In the first synchronization configuration, the oscillation is shown to be mainly controlled by the back and forth propagation of pressure waves in the oscillators' branches and feedback loops and its frequency can be estimated by the same simple relation as the one used for single oscillators. In the second synchronization configuration, the jet switching time is no more negligible compared to the pressure waves propagation time, leading to more complex oscillation dynamics.

1. Introduction

Even if flow control (FC) strategies can be employed for a wide range of applications including for example flow-induced noise reduction [1] or mixing in combustion chambers [2,3], the main field of investigation concerns flow separation control in order to reduce pressure drag on bluff bodies [4] or to increase lift on airfoils [5,6]. Active FC techniques drew researcher's attention due to their ability, unlike passive techniques, to be adapted to operating conditions. For this reason, the study of actuators for active flow control has been in focus for many decades [7–9].

By blowing or suction in a steady or unsteady manner, fluidic actuators aim to re-energize the flow in the boundary layer by enhancing the momentum in the vicinity of the wall. Zero-net-mass-flux (ZNMF) fluidic actuators are able to alternate between blowing and suction using a periodic motion generator. On the contrary, other types of actuators do not require any moving parts (*e.g.* continuous jet actuators [4] or sweeping jet actuators [10]) and appear to be more reliable and robust for harsh operating conditions.

As unsteady actuation appears to be a much more attractive strategy to improve FC system efficiency [11,12], fluidic oscillators seem to be good candidates for FC application compared to other types of fluidic actuators [7], both because they have no moving parts, and deliver periodic fluidic excitations. They can emit oscillating jets when supplied with a pressurized fluid. The fact that their oscillations are totally self-induced and self-sustained and only depend on the internal flow dynamics is a great advantage [13–15].

Among many concepts of fluidic oscillators detailed by Tesar [16], fluidic oscillators with single bistable amplifier and two feedback loops

Abbreviations: FC, Flow control; FBL, Feedback loop; OSC, Oscillator; HPCW, High pressure compression wave; LPEW, Low pressure expansion wave; ZNMF, Zero-net-mass-flux.

* Corresponding author at: Institut Clément Ader (ICA), Université de Toulouse, CNRS, INSA, ISAE-SUPAERO, Mines-Albi, UPS, Toulouse, France.
E-mail address: ahmad.batikh@icam.fr (A. Batikh).

https://doi.org/10.1016/j.sna.2024.115165
Received 12 May 2022; Received in revised form 4 August 2023; Accepted 7 February 2024
Available online 10 February 2024

Nomenclature

C_0	Speed of sound in air at 20 °C (m/s)
f	Oscillation frequency (Hz)
L_f	Feedback loop length (m)
u	Local velocity in the feedback loop (m/s)
U	Local velocity at the center of oscillators' outlet (m/s)
$\overline{U}$	Area-averaged velocity in the oscillators' branch inlet (m/s)
t	Time (s)
T	Oscillation period (s)
P_{atm}	Atmospheric pressure (Pa)
$\Delta P_{\mathrm{P-P}}$	Pressure difference between the control ports at the jet base (Pa)
$\Delta P_{\mathrm{A-A}}$	Pressure difference between the two main branches (Pa)
τ_t	Transmission time in one direction (s)
τ_s	Switching time (s)

recently received a great attention for flow control applications [17–20]. They have been widely used, since the 1970 s, as fluidic logic components or flowmeters [21–23]. Two versions of this type of oscillators have been developed. The first one has only one outlet in which a continuous but spatially oscillating jet can be generated [24–27], and is called sweeping jet oscillator. The other kind of oscillator has two outlets which can generate pulsing jets in opposite phases, and is called pulsing jet oscillator [17,18,28,29].

From a practical point of view, in order to apply this kind of fluidic oscillator to control the flow separation in a large scale, for instance on a wing, a series of actuators arranged in the area requiring flow control is needed. Gokoglu *et al.* [30] showed that synchronization improved the control authority of the array of oscillators when applied to air film cooling in turbines, while Shigeta *et al.* [31] observed that synchronized fluidic oscillator arrays were able to suppress the noise produced by a turbulent flow over an open cavity.

In the work of Aram *et al.* [32], large eddy simulations were carried out to study the phase delay effects between two identical fluidic oscillators on the flow control efficiency of a hump flow. And their results show that the flow control efficiency of synchronized fluidic oscillators is remarkable in which the whole recirculation separation region is eliminated, while different delayed phases lead to different control results. In the experimental studies on interactions between fluidic oscillators and main flow stream by Ostermann *et al.* [33] and Hossain *et al.* [34], it is found that the phase position of neighboring oscillator generates a major impact on the flow vortex along the main flow direction, which affects the overall separation control efficiency. All the above mentioned studies imply that the frequency and phase synchronization of a large fluidic oscillator array can generate an orderly vortex in the controlled flow region, so as to further improve the flow control efficiency.

To our knowledge, only a few studies have investigated the synchronization strategies of fluidic oscillators arrays in the literature. The first common strategy applied in these works is based on a shared inlet accumulator, as proposed by Gokoglu *et al.* [30], who tested numerically an array of sweeping jet oscillators (with one inlet and one outlet). The authors concluded that synchronous output jets could be obtained if the array is started from stillness. However, they were not able to experimentally synchronize, by controlling the inlet boundary conditions, an initially asynchronous array, because the array behavior was shown to be very sensitive to asymmetric perturbations and imperfections in the oscillators geometry. In the patents of Ciro *et al.* [35] and Koklu [36], new methods to synchronize an array of, respectively, pulsed jets and sweeping jet oscillators, have been proposed using the concept of shared feedback accumulator in addition to the shared inlet accumulator. In the first patent [35], the authors proposed to connect each feedback chamber of one oscillator side (*e.g.* left side) to the opposite feedback chamber of the next oscillator (*e.g.* right side) and so on. In the second patent [36], the author proposed, in addition to an inlet accumulator, to use a feedback plenum for the right sides and another one for the left sides to synchronize three sweeping jet oscillators. As a result, all jets from connected oscillators' outlets are synchronous in sweeping direction and have the same frequency. Tomac *et al.* [37,38] applied with success this concept to synchronize a pair of sweeping-jet oscillators for a wide range of operating conditions leading to exit jet Reynolds numbers ranging from 4250 to 34,000 and oscillation frequencies between 182 and 940 Hz. In addition to the experimental proof of concept, their numerical analysis highlighted the complex flow interactions in the shared feedback channels leading to the outlet jets synchronization. This idea of shared feedback plenum was also extended to a back-to-back configuration by Sundström *et al.* [39,40] or a stacked configuration by Tomac *et al.* [41,42] to synchronize an oscillator pair. In the patent of Seifert *et al.* [43], the authors suggested two strategies to synchronize a pair or more of suction and blowing oscillators, as presented in Fig. 1 (a fluidic ejector, not represented in the figure, supplying a fluidic diverter valve with two outlets in addition to two control ports). Their first strategy consists in connecting oscillators in a parallel configuration, which means that all control ports of each side are connected to the same control flow source (Fig. 1-a). On the contrary, the second strategy consists in connecting each control port of an oscillator (right or left side) to the same port of the next one (Fig. 1-b). According to the patent, the oscillator array operates uniformly with a limited oscillation frequency and amplitude deviations between 1 % and 20 %, and an oscillation phase offset ranging from 0.1 to 0.4 rad. Finally, Bauer *et al.* [44] proposed two ways to control the switching process of an array of fluidic diverters connected to a pressurized air source. The first method is based on a periodic pneumatic signal obtained by solenoid valves and used at the diverters control ports. In the second method, the pneumatic periodic control signal is obtained from a 1st stage fluidic oscillator connected to the control ports of the second stage oscillators, as shown in Fig. 2. Even if these two methods make it possible to synchronize the generated pulsed jets, the system in the second method seems to be more complex and, for the first switching control method, abandon the great advantage of reliability of fluidic oscillators due to the use of solenoid valves.

All previously described works clearly highlight that the way in which actuators are connected has a great impact on their collective behavior.

However, these studies were either dealing with sweeping jet fluidic oscillators, whose switching mechanism is mainly controlled by the internal design of the oscillator and the mass flow through the feedback loops, or concerned pulsed jets oscillators but with an additional control system for the synchronization of the output jets.

To our knowledge, there are no studies on the synchronization of bistable fluidic oscillators, whose switching mechanism is mainly linked to the length of their feedback channels as it will be shown in the next section. As the synchronization strategy adopted in this work is based on interconnections of the feedback loops of adjacent oscillators in the array of actuators, an in-depth study of the internal flow dynamics of the oscillators is needed in order to understand how the switching mechanism is modified by these interconnections, and thus to be able to propose guidelines for actuator array design to match the FC requirements.

The present paper is organized into five sections. Following the introduction and literature review in Section 1, a reminder of the dynamics of a typical bistable oscillator is presented in Section 2. Then, in Section 3, the experimental configurations tested during this work are detailed. The analysis of synchronization strategies is developed in Section 4. Finally, a computational analysis is conducted and detailed in Section 5 to determine whether or not the synchronization methods chosen have affected the operating dynamics of the connected oscillators. The paper ends with a conclusion and perspectives on the use of an

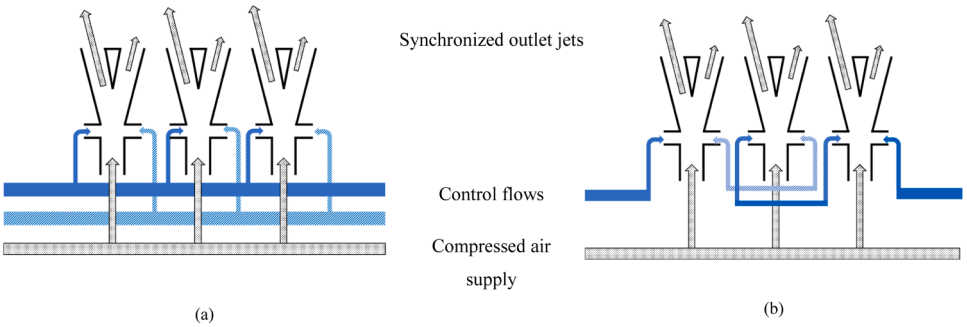

Fig. 1. Synchronization strategies according to [43].

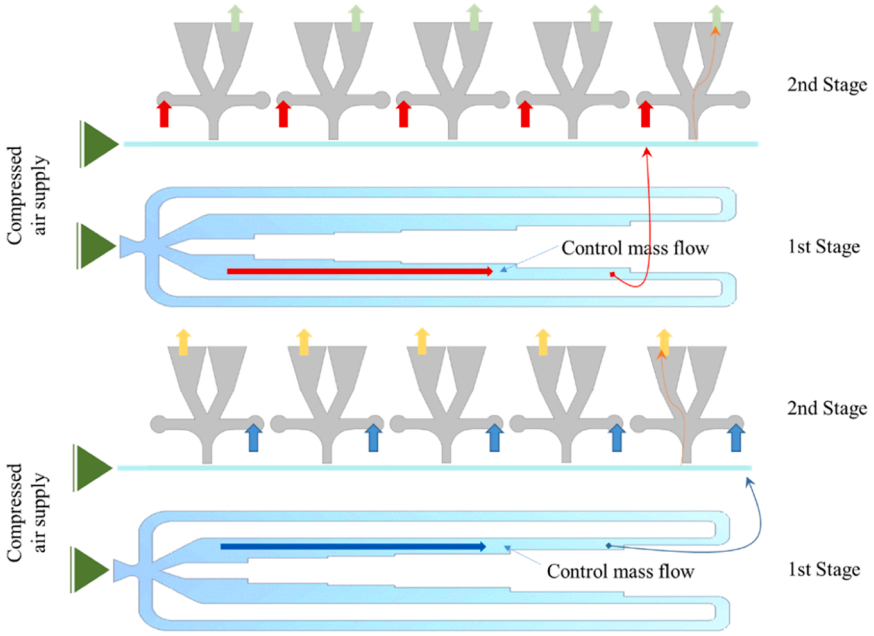

Fig. 2. Two-stage fluidic actuators according to [44].

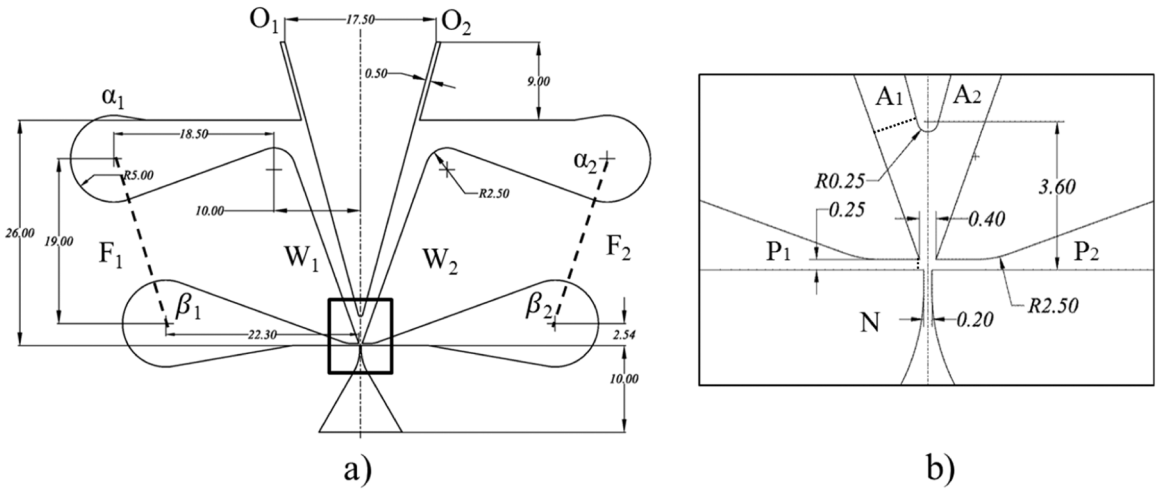

Fig. 3. Sketch and key dimensions (in mm) of the experimental oscillators, represented without their FBL connecting α_1 to β_1 and α_2 to β_2; a) global view, b) zoomed view.

array of synchronized fluidic oscillators to control flow separation on a ramp.

2. Operating dynamics of a typical fluidic oscillator

In previous studies [45,46], a pulsing jet fluidic oscillator for flow separation control was proposed and characterized. It was based on the geometry of the mono-stable oscillator developed by Khelfaoui *et al.* [47] but with two feedback loops (FBL) and outlet channels, as shown in Fig. 3, which includes a detailed view of the "switching" region. This prototype is basically composed of a nozzle which throat is 0.2 mm in width, two changeable feedback loops F_1 and F_2 and two outlets O_1 and O_2. The depth of the device is 10 mm, which is much larger than the width of the internal channels thus ensuring a quasi-2D behavior of the internal flow. The FBL are made with changeable plastic tube, 4 mm in diameter, connecting connectors α to β in each side. Its behavior is based on the Coanda effect [48]: the jet issuing from nozzle N attaches one of the two walls W_1 or W_2. The attachment to either wall W_1 or wall W_2 depends on the initial conditions or is the result of specific actions on the jet. Without feedback loops and for large enough outlet sections, the flow would stay attached to wall W_1 or wall W_2 and, accordingly, would exit through the corresponding outlet, O_1 or O_2, respectively. With feedback loops, when the jet is attached to wall W_1, due to the hydraulic restriction at outlet O_1, a part of the flow is deviated towards the feedback loop F_1, which in turn yields a pressure increase in the left side of the device. This pressure increase, coupled with a lateral perturbation to the main jet induced by a pressure difference between oscillator main branches A_1 and A_2, provokes the jet switching to the other side. Following the jet switching, the same phenomenon develops in the right side of the oscillator and results in a self-sustained oscillating behavior, with a pulsed flow alternatively exiting through outlets O_1 and O_2.

The operating dynamics of a typical fluidic oscillator, and specially its frequency response, has been studied in detail in a previous paper [46]. Its findings are presented here briefly in order to emphasize the modification of flow patterns induced by the synchronization. More detailed information can be found in the original work.

It was found that the jet oscillation frequency has a direct relationship with the forth and back propagation of the pressure waves in the branches and the feedback loops. The switching of the jet results from both the pressure difference between the control ports (P_1 and P_2 in Fig. 3b) at the jet base and the pressure difference between the two branches (A_1 and A_2 in Fig. 3b). When the jet is attached to one branch, *e.g.* on the left side, a high-pressure compression wave (HPCW) propagates along the left feedback loop F_1, which results into the rise of the local pressure. The HPCW propagation velocity is $C_o + u_1$, where C_o is the speed of sound and u_1 is the local fluid velocity in front of the wave. At the same time, on the right side, there is a low-pressure expansion wave (LPEW) propagating along the right FBL. When these two pressure waves arrive at the jet base after almost a quarter of period, the pressure difference between these two control ports reverses. However, this pressure difference is not able to initiate the main jet switching, though it makes the main jet very unstable. Hereafter, the HPCW is reflected back and continues propagating along the left FBL with a velocity $C_o - u_2$, where u_2 is the local fluid velocity in front of the reflected wave. This reflected HPCW increases the local pressure to a higher level. As it reaches the left branch inlet section, the main jet is forced to switch to the right side and another half period begins.

The oscillation period can thus be estimated by the following relation:

$$T = \frac{1}{f} = 2\left(\frac{L_f}{C_o + u_1} + \frac{L_f}{C_o - u_2} + \tau_s\right) \quad (1)$$

where L_f is the feedback loop length (from section A to section P on Fig. 3-b, including the connecting tube length and the internal channel length), while τ_s is the jet switching time.

The wave propagation patterns and switching dynamics have been confirmed experimentally in a more recent paper [49], using fast pressure sensitive paints.

3. Synchronization strategies and experimental configuration

To study the synchronization of the oscillators in the simplest configurations, experiments were first carried out on two identical interconnected oscillators, Osc.1 and Osc.2. The detailed dimensions of these two symmetrical devices are given in Fig. 3. The depth of the central part was 10 mm. Plastic tubes were used to form feedback loops (*a*, *b*, *c*, and *d*) linking connectors α_i and β_i.

Two interconnection configurations, shown in Fig. 4, were tested to synchronize these two oscillators and led to an oscillatory behavior of the actuators.

In the first configuration (Fig. 4a), the left upper connector α_1 of Osc.1 was linked to its own left lower connector β_1 by FBL *a*, and the right upper connector α_2 of Osc.2 was linked to its own right lower connector β_2 by FBL *d*. On the other hand, the right upper connector of Osc.1 was linked to the left lower connector of Osc.2 by FBL *b* and the right lower connector of Osc.1 was linked to the right upper connector of Osc.2 by FBL *c*.

In the second configuration (Fig. 4b), the left upper connector of Osc.1 was linked to the left lower connector of Osc.2 by FBL *a*, while the left upper connector of Osc.2 was linked to the right lower connector of Osc.1 by FBL *c*. The same interconnection pattern was used for the right connectors of both oscillators.

All tubes used for interconnections (*a*, *b*, *c*, and *d* in Fig. 4) had a length of 500 mm and an inner diameter of 4 mm. The FBL length L_f was then the sum of the tube length (500 mm) and the internal channel length (86 mm). Both oscillators' inlets were connected to the same pressure tank.

Two pressure sensors (Endevco 8506–2, gauge pressure range 0–14 kPa, resonance frequency 35 kHz) were placed in front of right outlets O_2 of both oscillators at a distance of 0.5 mm from the oscillators' exit slots. It was verified that the frequency of the acquired signals was not influenced by this distance. The sampling frequency was set to 25 kHz in both cases and the signals were recorded simultaneously during 10 s

4. Experimental results

Firstly, the frequency response of each oscillator working independently was measured. The inlet pressure P_i ranged from 0.12 to 0.27 MPa. Frequency deviations between the two single oscillators can be clearly observed in Fig. 5, though the difference stays in the range 3 to 10 Hz, *i.e.* about 2 to 6 % of the average frequency, depending on the supply pressure. These deviations are probably due to small differences in the oscillators' internal geometry (linked to the fabrication process) and in the tube lengths of the feedback loops.

The frequencies obtained for the two synchronized configurations are also shown in Fig. 5. With the first synchronization configuration (see Fig. 4a), the working frequency of both oscillators is $f_1 \approx 155$ Hz, which is very close to the frequencies obtained when the oscillators work separately. More precisely, there is a slight difference between the natural frequencies of each single oscillator, as previously explained, and the frequency of the synchronized oscillators in the first configuration is between the natural frequencies of Osc.1 and Osc.2 working alone. The auto-correlation and cross-correlation of the pressure signals from Osc.1 and Osc.2 shown in Fig. 6 permit to calculate the phase lag between the two pulsed jets in the first configuration, $\Delta T_1 = 0.46T_1$, close to half a period.

The frequency obtained with the second synchronization configuration (see Fig. 4b) is $f_2 \approx 105$ Hz, which is much smaller than that of the oscillators working independently. This frequency change implies that the oscillator's working dynamics in this synchronized case is very different from that in the separated case.

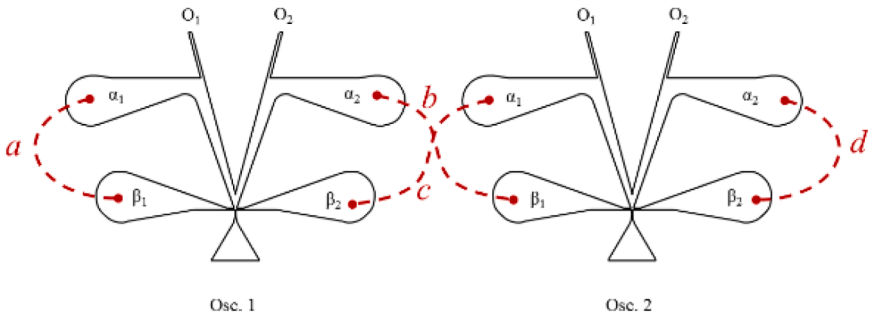

a) Configuration 1

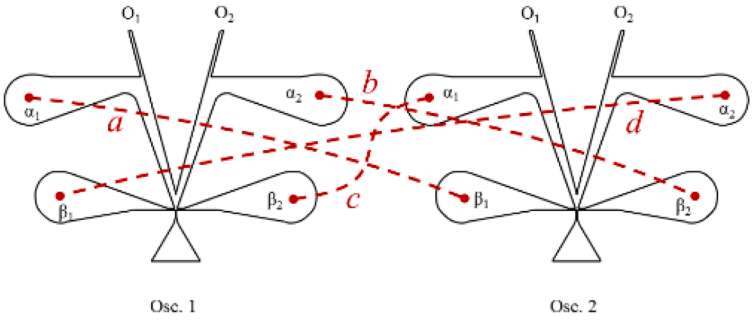

b) Configuration 2

Fig. 4. Two interconnection configurations leading to the synchronization of the two oscillators.

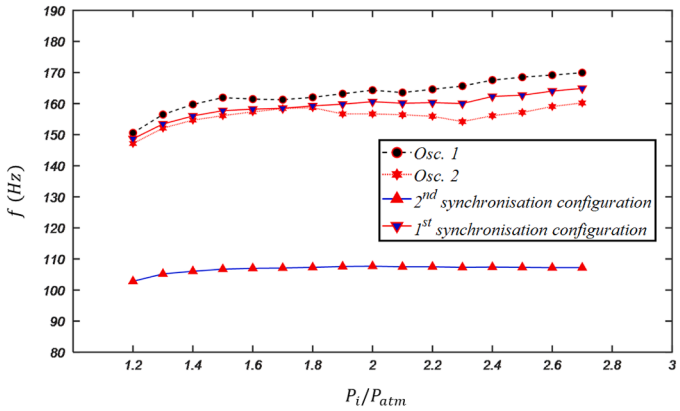

Fig. 5. Frequency responses of Osc.1 and Osc.2 working independently and frequencies obtained with different synchronization methods.

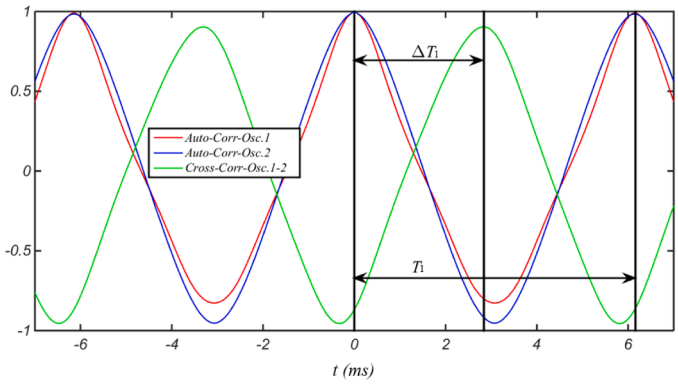

Fig. 6. Auto-correlation and cross-correlation sequences of the experimental pressure signals from Osc.1 and Osc.2 – 1st synchronization configuration.

A sample of auto-correlation and cross-correlation of the pressure signals is also shown in Fig. 7. The phase lag in this case is $\Delta T_2 = 0.253T_2$, *i.e.* approximately a quarter period.

5. Numerical analysis of the flow patterns inside the fluidic oscillator

In order to better understand the physical mechanisms controlling the oscillation dynamics in both configurations, the internal flow patterns were investigated with the help of computational fluid dynamics (CFD) analysis. The same computational method and settings as those used in [46] were applied. The main purpose of the simulations presented in this section was to analyze the synchronization dynamics, rather than the role of the FBL length which has a linear relationship with the oscillation frequency exploited in Eq. (1), as demonstrated in [46]. Thus, in order to reduce the simulation cost, the FBL length in the

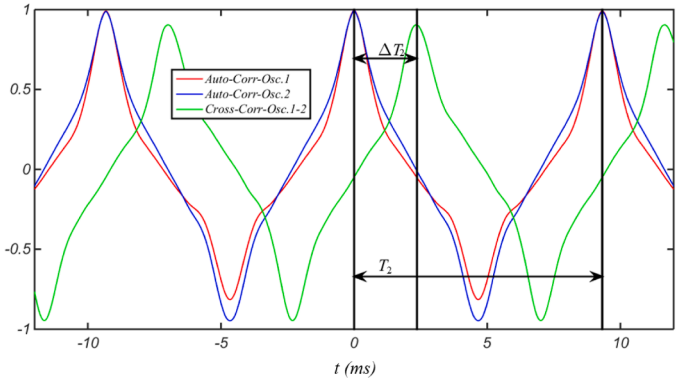

Fig. 7. Auto-correlation and cross-correlation sequences of the experimental pressure signals from Osc.1 and Osc.2 – 2nd synchronization configuration.

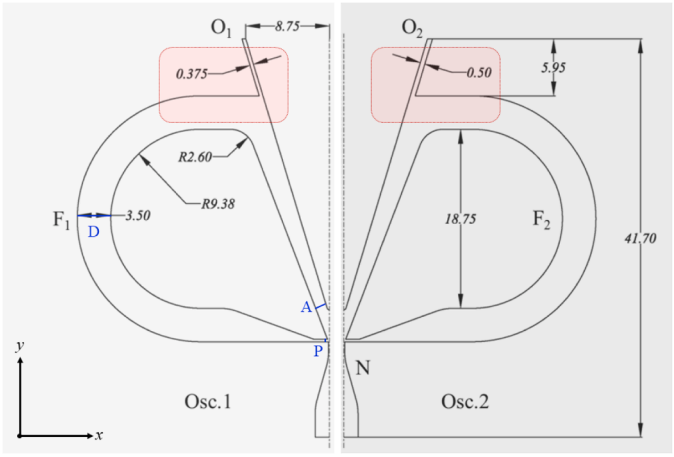

Fig. 8. Sketch and overall dimensions in mm of the two simulated oscillators, Osc.1 and Osc.2. Only the half part of each symmetrical oscillator is represented.

numerical model was chosen much shorter than in the experimental configuration, as shown in Fig. 8. Consequently, a qualitative -but not quantitative- comparison is possible between numerical results presented in Section 5 and experimental results from Section 4.

The open source CFD code OpenFOAM has been chosen to implement the 2D numerical simulations for its ability to deal with complex geometries using finite volume method and its high parallel computation capability. The governing equations are compressible Navier-Stokes equations in their conservative form. In the following series of simulations, the sonicFoam solver was used with 2nd order upwind spatial discretization schemes and a backward 2nd order temporal discretization scheme. The absolute total inlet pressure was set to 0.2 MPa, and an outlet static pressure of 0.1 MPa was imposed at the external boundaries of a rectangular domain with an area of 100×60 mm^2 placed at the oscillators exits to allow the pulsed jets development. The turbulence model was the realizable k-epsilon model. With a time step of 4×10^{-9} s, the maximum local Courant Number was limited to 0.3. The grid density at the wall permitted to obtain an average value of the dimensionless wall distance y^+ of the order of 10, compatible with the used standard wall function. The mesh files were generated using the software GAMBIT and only consisted of quadrangle cells in order to get high mesh quality. The total cell number was 1.2×10^5, with 20 nodes in the throat part and 15 nodes in both outlet sections. The working fluid was air, considered as an ideal gas with the following properties: molar mass $M = 28.9$ g/mol, specific heat capacity at constant pressure $c_p = 1005$ J kg^{-1} K^{-1}, dynamic viscosity $\mu = 1.8 \times 10^{-05}$ Pa s, and Prandtl number $Pr = 0.7$. In order to reach a steady periodic behavior, at least ten periods were simulated in each case.

Before starting the analysis, an elementary time τ_t, which is the transmission time of the pressure wave through the feedback loop in one-way (go or return), is defined:

$$\tau_t = \frac{L_f}{C_o} \approx \frac{L_f}{C_o + u_1} \approx \frac{L_f}{C_o - u_2} \tag{2}$$

as u_1 and u_2 are small compared to C_o and can be neglected.

Moreover, the switching time τ_s is usually negligible compared with the whole period T. Thus, the oscillation period T, given in Eq. (1), can be roughly predicted by a simpler relationship:

$$T = 2\left(\frac{L_f}{C_o + u_1} + \frac{L_f}{C_o - u_2} + \tau_s\right) \approx 2(\tau_t + \tau_t + \tau_s) \approx 4\tau_t \tag{3}$$

5.1. Simulation of two separated oscillators

In order to reproduce numerically the small differences in the working frequencies observed experimentally with the prototypes, all internal dimensions of these two oscillator models, given in Fig. 8, were identical, except the outlet width which was set to 0.375 mm for Osc.1 while it was kept to 0.5 mm as in the original design for Osc.2.

As the FBL length L_f (*i.e.* the distance between Sections A and P) is here equal to 75.62 mm, an oscillation frequency $f_{0-Eq.(2)} = \frac{340}{4\times75.62\times10^{-3}} = 1124$ Hz can be expected from Eqs. (2) and (3).

The simulated temporal evolutions of the velocity in the *y*-direction, U_y, in the center of left outlets O_1 of both oscillators, are compared in Fig. 9. It can be clearly observed that the two oscillators have slightly different frequencies. In time $t_0 = 15.25$ ms, they reach the maximum Uy in same phase, while about $\Delta t = 0.09\ T$ phase lag appears after 5 periods. More precisely, Osc.1 has an oscillation frequency $f_{0-Osc.1} = 1104$ Hz while Osc.2 has a frequency $f_{0-Osc.2} = 1127$ Hz, which are both very close to the value $f_{0-Eq.(2-3)} = 1124$ Hz estimated with simple Eqs. (2) and (3).

5.2. Simulation of two oscillators synchronized according to 1st interconnection configuration

Fig. 10 presents a sketch of the 1st simulated configuration. In order to facilitate the analysis of the oscillator behavior, three representative sections, noted (A, D, P), have been selected: they represent the branch inlet, the loop center, and the control port, respectively. Subscript *a* is relative to the sections along tube *a* connecting the left control port and the left branch of Osc.1; Subscript *b* is relative to the sections along tube *b* connecting the right control port of Osc.1 to the left branch of Osc.2; Subscript *c* is relative to the sections along tube *c* connecting the left control port of Osc.2 to the right branch of Osc.1, and Subscript *d* is relative to the sections along tube *d* connecting the right control port and the right branch of Osc.2. In this 2-D simulation, a translational periodic boundary condition is implemented to virtually connect Sections D_b and D_c for each oscillator.

In Fig. 11, where the velocities U_y in the center of the left outlet slots O_1 in both oscillators are compared, it can be seen that they are successfully synchronized with a frequency $f_1 = 1107$ Hz, very close to the estimated value from Eqs. (2) and (3). The phase difference is equal to $\Delta T_1 = 0.384T_1 \approx \frac{3}{8}T_1$, which is a bit smaller than the phase difference of $0.46T_1$ found during the experiments. Here, $T_1 = \frac{1}{f_1}$ is the period of the oscillation.

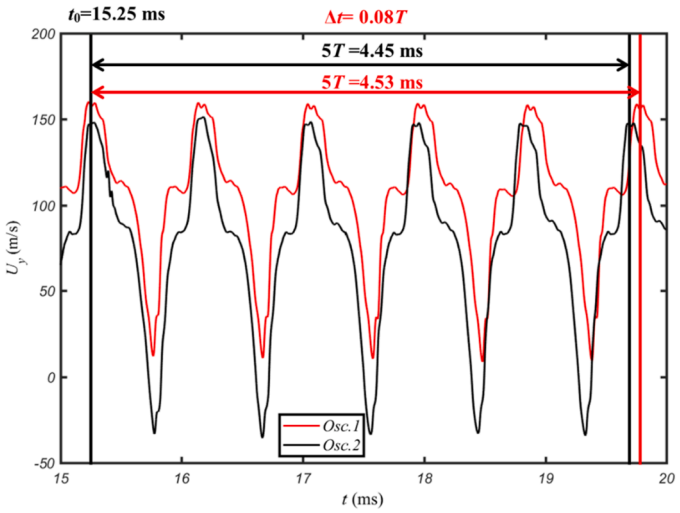

Fig. 9. Evolution with time of velocity U_y at the center of the left outlets O_1 of Osc.1 and Osc.2 working separately.

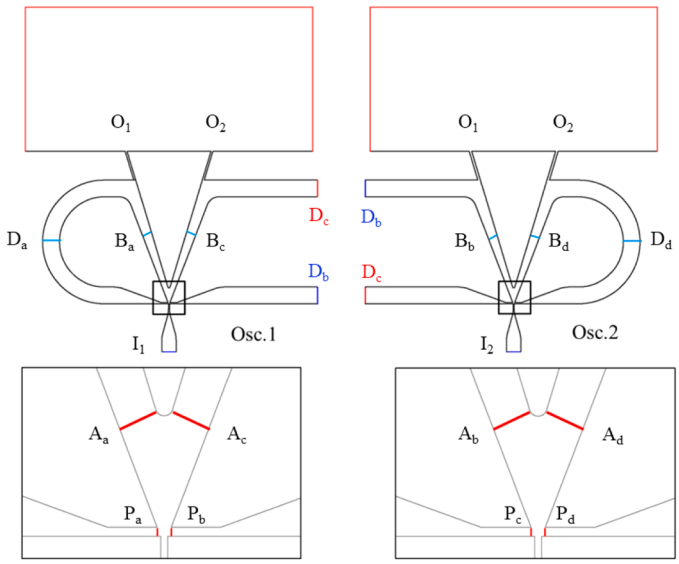

Fig. 10. Sketch of the simulated pattern for the 1st synchronization configuration.

These two results indicate that the synchronization dynamics is not significantly different from the one observed in the experimental case, despite a much smaller FBL and consequently a much higher frequency in the numerical case, confirming that the simulation results can be used to analyze the underlying synchronization mechanisms.

The transmission time τ_t will be used thereafter in order to facilitate the analysis of the synchronization dynamics. According to Eq. (2), $\tau_t = \frac{L_f}{C_0} = 0.224$ms.

Fig. 12 shows the phase portrait obtained from the velocities Uy at the center of the left outlets O1 of Osc.1 and Osc.2 synchronized according to the 1st configuration. It is evident that the self-sustained oscillation mechanism remains stable, as the trajectory overlaps for each period.

Several critical times are chosen for better analyzing the flow patterns inside the oscillators and explaining the synchronization dynamics. These times are defined according to the evolution of area averaged velocity $\overline{U}_y$ in the branch inlet sections of each oscillator, which are shown in Fig. 13.

- t_0 is defined when the main jet in Osc.1 is switching from the left branch to the right one, *i.e.* when the initially positive velocity $\overline{U}_y$ in the left branch inlet section A_a becomes equal to the initially negative velocity $\overline{U}_y$ in the right branch inlet section A_c. This time is assumed to be the beginning point of an oscillation period in our analysis. In the same time, the main jet in Osc.2 is attached to the right branch, which is indicated by the positive value of $\overline{U}_y$ in section A_d, while $\overline{U}_y$ is negative in section A_b.
- t_1 is chosen when the main jet in Osc.2 is switching from the right branch to the left one, while the main jet in Osc.1 is attached to the right branch.
- t_2 and t_3 are defined as one transmission time τ_t later than t_0 and t_1, respectively: $t_2 = t_0 + \tau_t$ and $t_3 = t_1 + \tau_t$
- t_4 is defined as the mid-point of a period: $t_4 = t_0 + 0.5T_1 \approx t_0 + 2\tau_t$, as τ_t is close to a quarter of period.

In the second half-period, it can be clearly observed that the pressure and velocity variation profiles are similar to those in the first half period, thus, detailed analysis is focused on the first half period.

Fig. 14 presents the evolution with time of the pressure differences in Osc.1 between the branch inlet sections A_a and A_c, $\Delta P_{Aa\text{-}Ac}$, and between the control port sections P_a and P_b, $\Delta P_{Pa\text{-}Pb}$, together with their counterparts in Osc.2, $\Delta P_{Ab\text{-}Ad}$ and $\Delta P_{Pc\text{-}Pd}$.

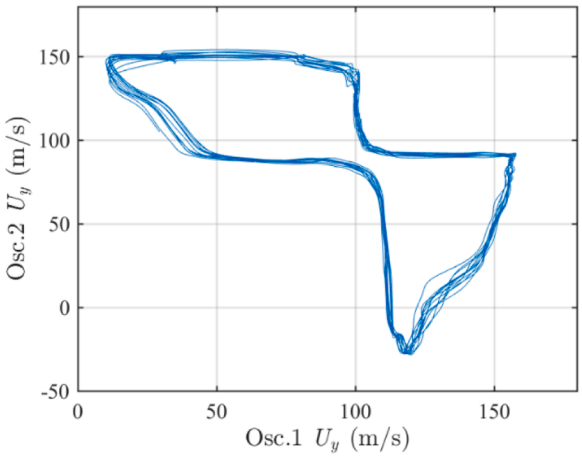

Fig. 12. Phase portrait of the velocity Uy at the center of the left outlets O1 of Osc.1 and Osc.2 synchronized according to the 1st configuration.

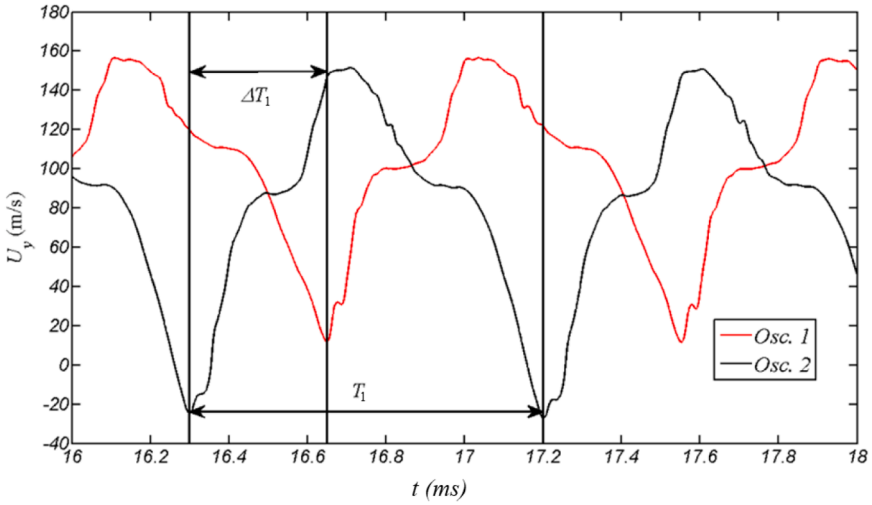

Fig. 11. Evolution with time of the velocity U_y at the center of the left outlets O_1 of Osc.1 and Osc.2 synchronized according to the 1st configuration.

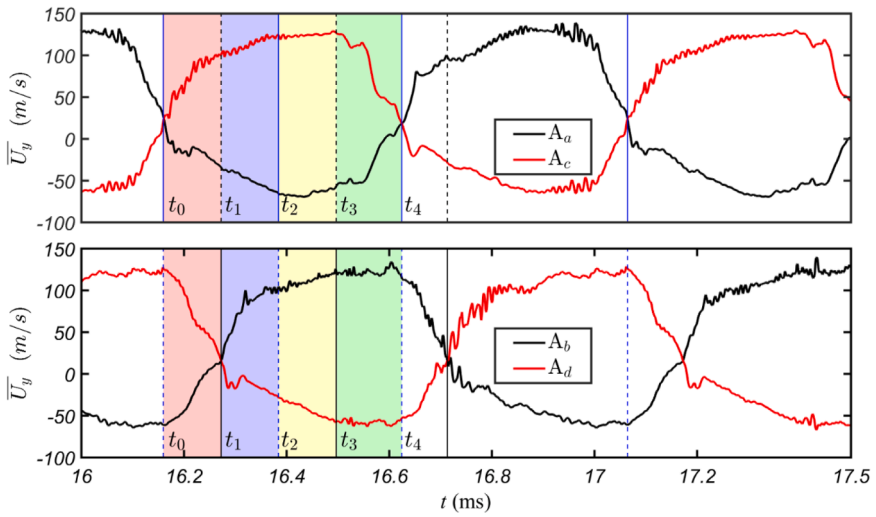

Fig. 13. Evolution with time of the average velocity $\overline{U}_y$ in the branch inlet sections A of both Osc.1 (sections A_a and A_c, upper figure) and Osc.2 (sections A_b and A_d, lower figure). Time intervals between the critical times t_0, t_1, t_2, t_3 and t_4 are identified by different background colors for a better visualization.

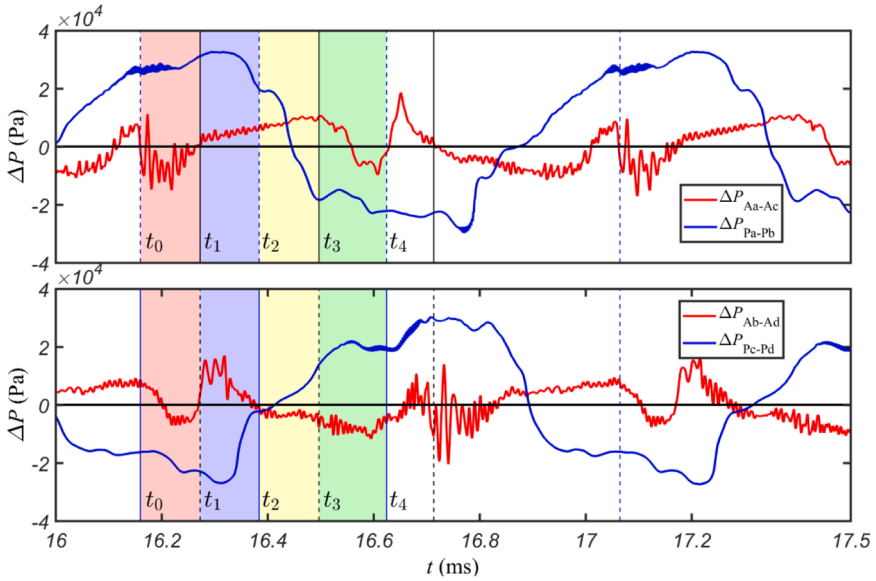

Fig. 14. Evolution with time of the pressure differences between the control ports P and branch inlets A in each oscillator (upper figure: Osc.1 and lower figure: Osc.2).

For each of the specific times defined above, a simplified sketch showing the main jets direction and the propagation of pressure waves along the feedback loops in each oscillator is also presented in Fig. 15. The pressure levels in sections A, D and P in each side of each oscillator are schematically represented by a level in a cylinder: an empty cylinder means that the pressure at this time has the lowest value calculated over the whole period, while a fully filled cylinder means that the pressure has reached its highest value. These pressure level representations are relative: the maximum pressure level in section A is not necessarily higher than the minimum one in section D.

Time t_0: from Fig. 14, it can be observed that at t_0, the pressure in section P_a is 27 kPa higher than that in section P_b, while the pressure in section A_a is also a slightly higher than that in section A_c. The combination of these two pressure differences provokes the switching of the main jet in Osc.1 from the left branch to the right one. Concerning the jet in Osc.2, though the pressure in section P_d is 20 kPa higher than that in section P_c, the main jet is still attached to the right branch since the pressure in section A_d is still about 7 kPa lower than that in section A_b. This is consistent with the fact, demonstrated in our previous works [46], that the jet switching mechanism in a single oscillator is provoked by the combination of the pressure differences between the control ports and between the branches.

Time t_1: from t_0 to $t_1 \approx t_0 + 0.125T_1$, a HPCW propagates along tube c, from A_c to D_c, and a LPEW also moves from A_a to D_a due to the entrainment effect of the main jet. At the same time, in Osc.2, a HPCW propagates from D_d to A_d and provokes at t_1 the switching of the main jet from the right side to the left one.

Time t_2: At $t_2 = t_0 + \tau_t$, the HPCW in tube c arrives in section P_c, which is the left control port of Osc.2, leading to a pressure augmentation up to the highest value. Similarly, the LPEW in tube a arrives in section P_a leading to a pressure decrease down to its lowest value. In the case of a single oscillator, the pressure in one of the control ports would decrease simultaneously when the pressure increases in the other control port, leading to the inversion of the pressure difference and provoking a destabilization of the main jet. However, in this synchronized case, the pressure in P_b is maintained at its lowest level since the HPCW

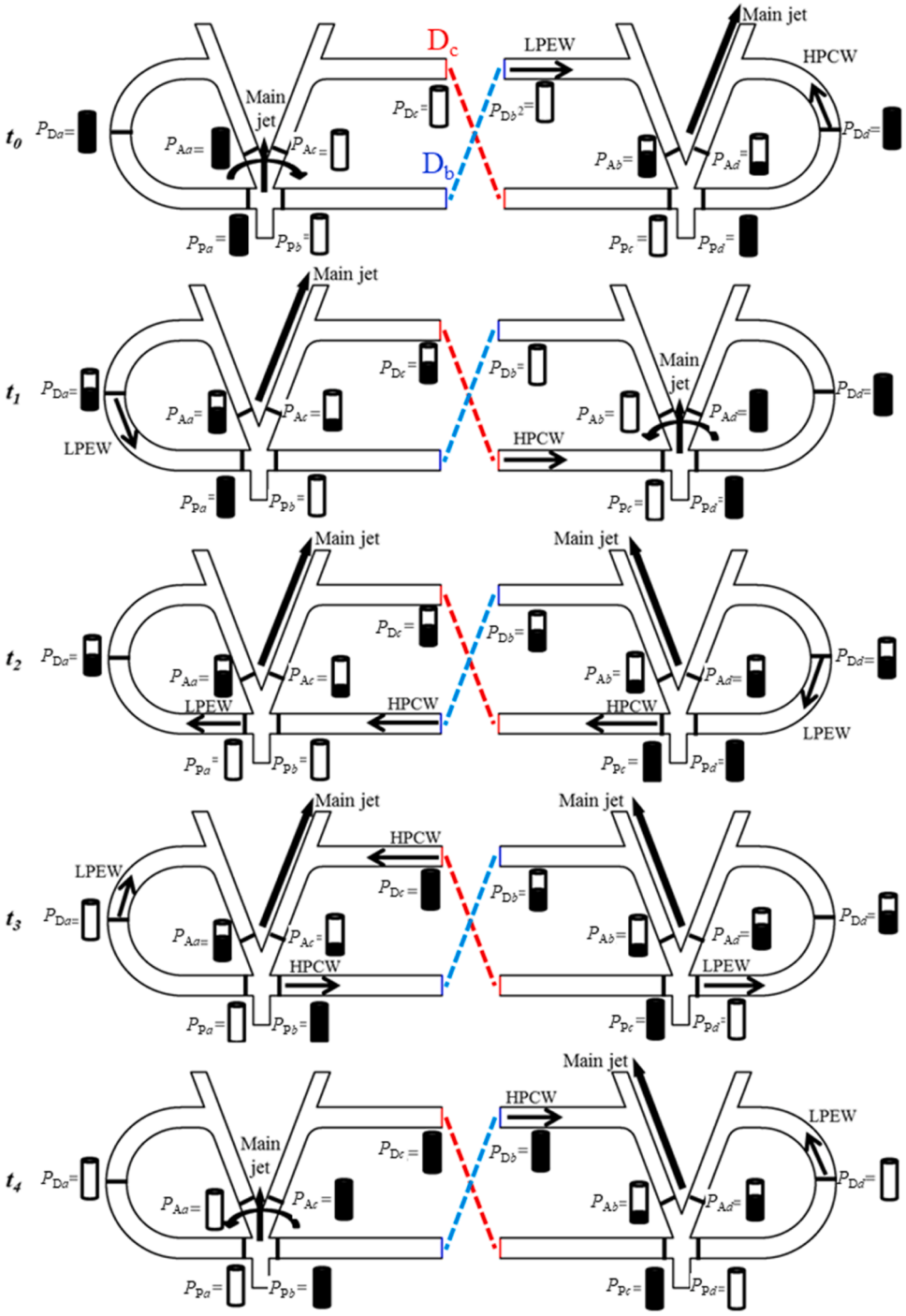

Fig. 15. Sketch showing the main jet directions and propagation of pressure waves along the feedback loops at each defined critical time; left side Osc.1, right side Osc.2.

in tube *b* needs additional time, 0.125 T_1, to reach P_b. Similarly, the pressure in P_d is maintained at its highest level since the LPEW in tube *d* also needs 0.125 T_1 to reach P_d. Thus, $\Delta P_{Pa\text{-}Pb}$ is still positive and $\Delta P_{Pc\text{-}Pd}$ still negative at time t_2, although their absolute values have decreased a lot compared to t_1 (*cf.* Fig. 15). Consequently, the main jets in both oscillators stay very stable, as it can be seen on the $\overline{U}_y$ evolution curves in Fig. 14.

Time t_3: At $t_1 + \tau_t$, the pressure differences $\Delta P_{Pa\text{-}Pb}$ and $\Delta P_{Pc\text{-}Pd}$ have changed their sign since the HPCW and the LPEW arrive in sections P_b and P_d, respectively. As the pressure difference $\Delta P_{Aa\text{-}Ac}$ is still positive, the main jet in Osc.1 does not switch but becomes unstable. The velocity $\overline{U}_y$ in section A_c begins to decline.

Time t_4: Just before $t_4 = t_0 + T_1/2$, the HPCW reflected from section P_c in tube *c* reaches section A_c: $\Delta P_{Aa\text{-}Ac}$ is negative and reaches its maximum absolute value. In combination with the large pressure difference $\Delta P_{Pb\text{-}Pa}$ at the control ports, this thus provokes the switching of the main jet in Osc.1 from the right side to the left one which occurs at t_4. The first half period is finished.

Due to the interconnection pattern, the frequency response is shown to be here independent from the phase lag between the two oscillators and is directly linked to the back and forth propagation of pressure waves in the branches and feedback loops. Therefore, in this

configuration, the synchronized oscillator reaches a switching frequency very close to that of the individual oscillator.

5.3. Simulation of two oscillators synchronized with the 2nd interconnection configuration

Fig. 16 presents a sketch of the simulated configuration. Three sections, noted (A, D, P) are selected in the same way as in the previous configuration. Here, subscript a is relative to the sections along tube a connecting the left control port of Osc.1 to the right branch of Osc.2; subscript b is relative to the sections along tube b connecting the right control port of Osc.1 to the left branch of Osc.2; subscript c is relative to the sections along tube c connecting the left control port of Osc.2 to the left branch of Osc.1, and subscript d is relative to the sections along tube d connecting the right control port of Osc.2 to the right branch of Osc.1. In this 2-D simulation, translational periodic boundary conditions were implemented to virtually connect sections D_a, D_b, D_c and D_d defined on each oscillator.

In Fig. 17, computed velocities U_y at the center of the left outlet slot O_1 in both oscillators are compared and it can be seen that they are synchronized successfully with a frequency $f_2 = 1/T_2 = 88$ Hz, which is much lower than the value estimated from Eqs. (2) and (3). This frequency is also very similar to that observed experimentally. In addition, the phase difference is equal to $\Delta T_2 = 0.24T_2 \approx \frac{1}{4}T_2$, which is close to the phase difference $0.252\ T_2$ found during the experiments.

Fig. 18 shows the phase portrait of the velocity Uy at the center of the left outlets O1 of Osc.1 and Osc.2 synchronized according to the 2nd configuration. As for the first configuration, the overlapping of the trajectories drawn for different periods clearly evidence a stable and self-sustained oscillatory behaviour of the system.

With the same analysis procedure as in the previous configuration, several critical times are chosen according to the evolution of the area-averaged velocity $\overline{U}_y$ in each section A shown in Fig. 19.

- Time t_0 is chosen as the beginning point of a period when the main jet of Osc.1 is switching from the left branch to the right one.
- t_1 is defined as a transmission time τ_t later: $t_1 = t_0 + \tau_t$.
- t_2 is chosen when the main jet of Osc.2 is switching from the right branch to the left one. As the jet in Osc.2 switches at t_2 in the opposite direction (right to left) than the jet in Osc.1 at t_0 (left to right), thus, $t_2 = t_0 + (T_2/2 - \Delta T_2)$.

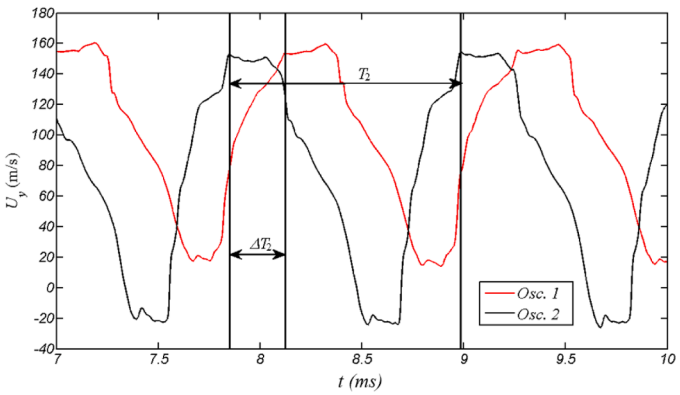

Fig. 17. Evolution with time of computed velocities U_y at the center of the left outlets O_1 of Osc.1 and Osc.2 synchronized according to the 2nd configuration.

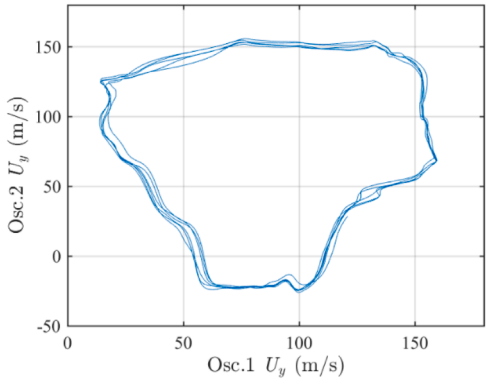

Fig. 18. phase portrait of the velocity Uy at the center of the left outlets O1 of Osc.1 and Osc.2 synchronized according to the 2nd configuration.

- t_3 is defined as $2\tau_t$ later than t_0, $t_3 = t_0 + 2\tau_t$.
- t_4 is defined as τ_t later than t_2, $t_4 = t_2 + \tau_t$.
- t_5 is chosen when the main jet of Osc.1 is switching from the right branch to the left one, marking the end of the first half period.

Fig. 20 presents the evolution of pressure differences between the

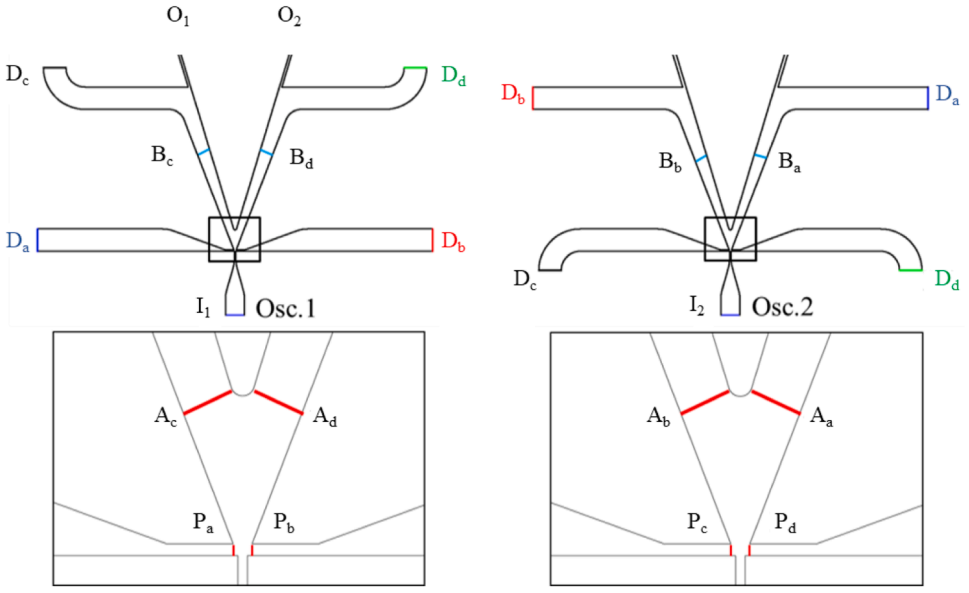

Fig. 16. Sketch of the simulated pattern for the 2nd synchronization configuration.

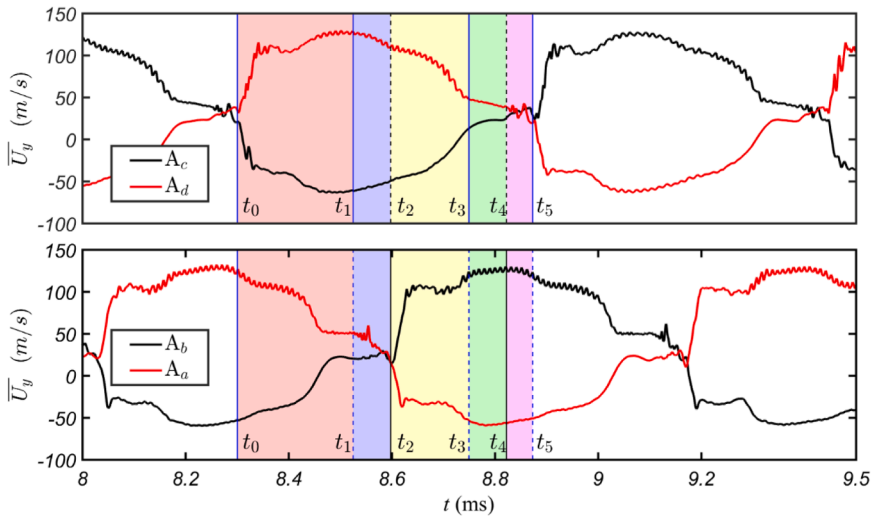

Fig. 19. Evolution with time of the area-averaged velocity $\overline{U}_y$ in the branch inlet sections of Osc.1 and Osc.2 - 2nd method of synchronization. Time intervals between the critical times t_0, t_1, t_2, t_3, t_4 and t_5 are identified by different background colors for a better visualization.

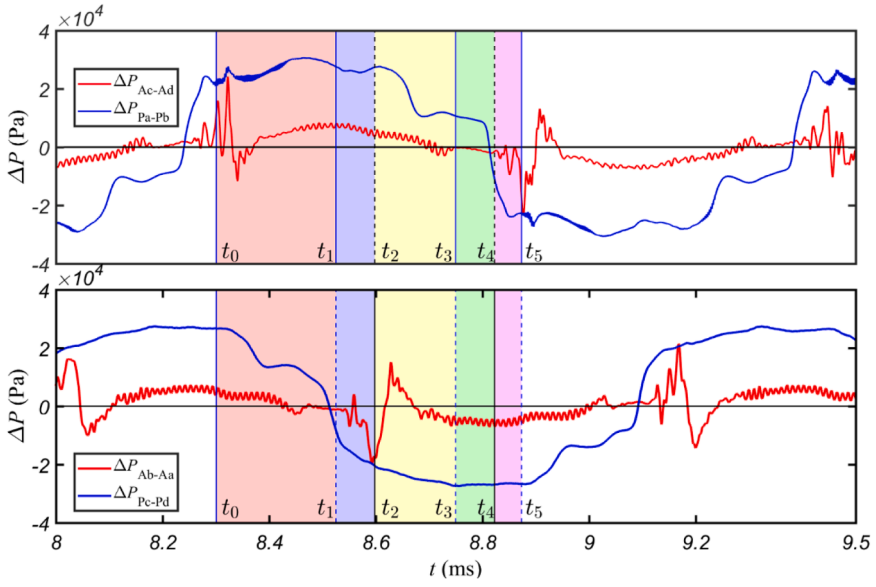

Fig. 20. Evolution with time of the pressure differences between the control ports P and branch inlets A in each oscillator in the 2nd method of synchronization.

branch inlet sections A_c and A_d, $\Delta P_{Ac\text{-}Ad}$, and between the control port sections P_a and P_b, $\Delta P_{Pa\text{-}Pb}$, in Osc.1, together with their counterparts in Osc.2, $\Delta P_{Ab\text{-}Aa}$ and $\Delta P_{Pc\text{-}Pd}$. Similarly to the previous configuration analysis, for each of the critical times defined above, a simplified sketch showing the main jets direction and the propagation of pressure waves along the feedback loops in each oscillator is also presented in Fig. 21.

Time t_0: from Fig. 20, it can be observed that at t_0, the pressure in section P_a is 21 kPa higher than that in section P_b, while the pressure in section A_c is also a little higher than that in section A_d. The combination of these two pressure differences provokes the switching of the main jet in Osc.1 from the left branch to the right one. In Osc.2, at this time, the main jet has been in the right branch for almost a quarter period (*cf.* Fig. 19). The pressures in both the left branch and the control port of this oscillator are higher than those in its right side, resulting in a stable attachment of the main jet to the right branch.

Time t_1: One transmission time τ_t later, the HPCW coming from section A_d along tube *d* arrives at the control port section P_d and reflects, while the LPEW propagates from A_c to P_c and then reflects. As a consequence, the value of $\Delta P_{Pc\text{-}Pd}$ decreases from 20 kPa to a negative value. However, the $|\Delta P_{Ab\text{-}Aa}|$ value is still too small to provoke the jet switching, which is in agreement with what has been shown on a single oscillator in the previous study.

Time t_2: The pressure difference $|\Delta P_{Ab\text{-}Aa}|$ between the branches of Osc.2 has now reached a value large enough to provoke, in conjunction with the large value of $|\Delta P_{Pc\text{-}Pd}|$, the switching of the jet in this oscillator. At this time, along tube *b*, the HPCW starts to propagate from section A_b, and along tube *a*, the LPEW starts to propagate from A_a. At the same moment, the fronts of the pressure waves in tube *d* (HPCW) and tube *c* (LPEW) are already in halfway along the tubes.

Time t_3: At this time, *i.e.* two transmission times after t_0, both the HPCW in tube *d* and the LPEW in tube *c* have reached back section A_d and section A_c, respectively, which makes the pressure difference between the branches $\Delta P_{Ac\text{-}Ad}$ changing from positive to a slightly negative value. However, the pressure difference at the control ports $\Delta P_{Pa\text{-}Pb}$ is still largely positive, which avoids the jet switching.

Time t_4: One transmission time τ_t later than t_2, the HPCW in tube *b* arrives in section P_b and the LPEW in tube *a* arrives in section P_a, provoking the destabilization of the main jet of Osc.1. This is particularly

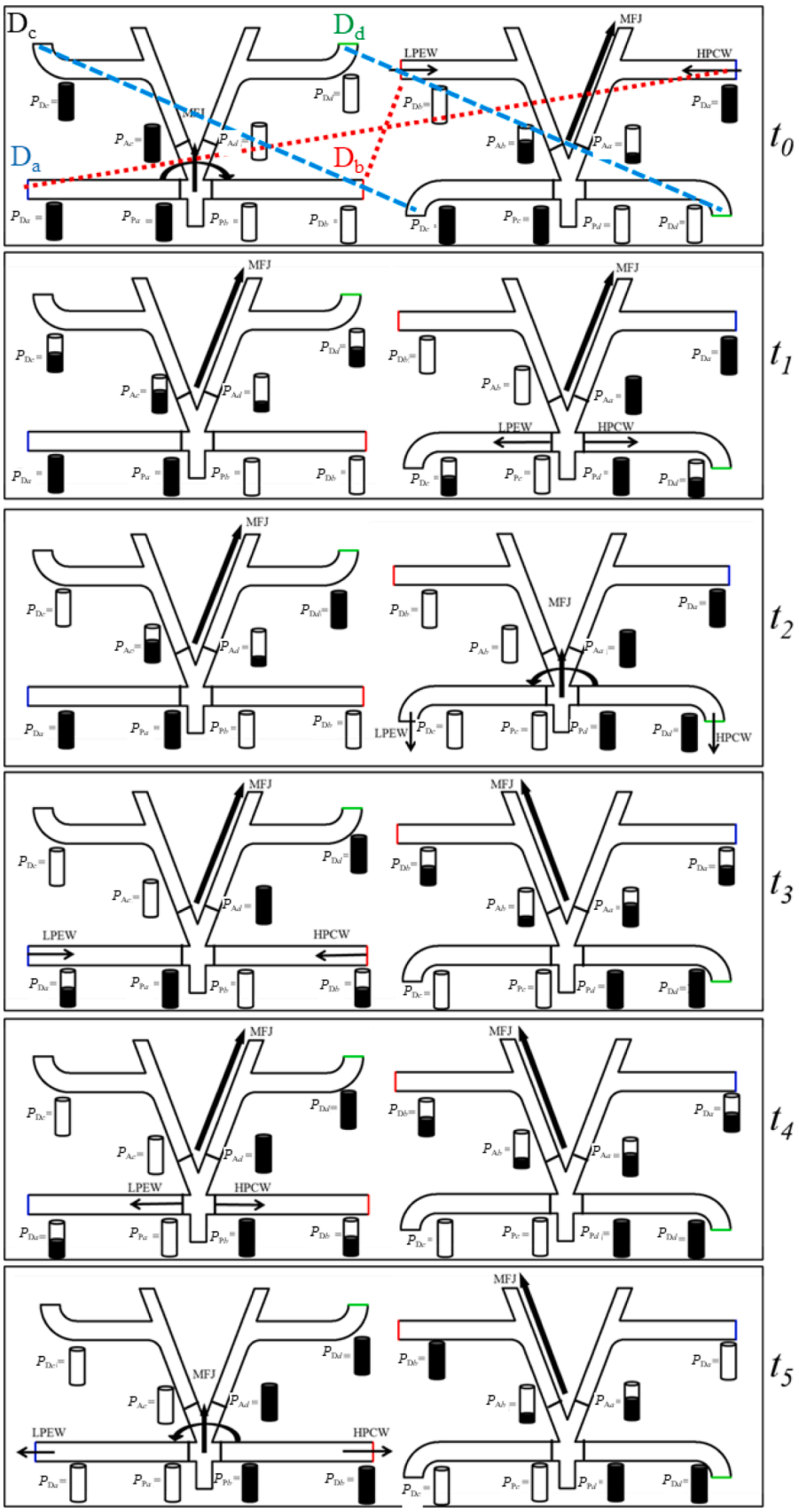

Fig. 21. sketch showing the main jet directions and propagation of pressure waves along the feedback loops at each defined critical time; left side Osc.1, right side Osc.2.

visible on $\overline{U}_y$ profiles in sections A_c and A_d: these 2 velocities are indeed very close and very perturbed between t_4 and t_5. A similar behavior can be observed for the $\overline{U}_y$ profiles in sections A_a and A_b between t_1 and t_2, in relation with the jet switching in Osc. 2, as well as just before t_0 for Osc.1.

Time t_5: The conjunction of the two pressure differences $\Delta P_{Pa\text{-}Pb}$ and $\Delta P_{Ac\text{-}Ad}$ provokes the switching of the jet in Osc.1. The time difference t_5 - t_4 can be related to the deflection time in Osc.1. Similarly, the time difference $t_2 - t_1$ can be related to the deflection time in Osc. 2.

From the above analysis, it can thus be observed that the switching time τ_s plays an important role in the oscillation dynamics, unlike for the first synchronization method where this switching time was found to be negligible compared to the half period. In the second synchronization method here studied, the switching time τ_s not only represents approximately one fourth of the transmission time τ_t but also appears twice in the calculation of the half-period (*cf.* Figs. 19 and 20):

$$T_2/2 = (t_1 - t_0) + (t_2 - t_1) + (t_4 - t_2) + (t_5 - t_4) = 2\tau_t + 2\tau_s \quad (4)$$

In addition, the phase lag, ΔT_2, is equal to one fourth of the oscillation period.

$$\Delta T_2 = (t_1 - t_0) + (t_2 - t_1) = \tau_t + \tau_s = T_2/4 \quad (5)$$

It is not yet clear why the switching time is so large in this configuration. It could be due to an additional time needed to empty completely the feedback loop on the low-pressure side (see for instance the evolution of the pressure in section D_a between times t_4 and t_5 in Fig. 21). Additional experimental investigations are however needed, using for example the same approach as in [49], for an in-depth analysis of the physical mechanisms controlling the jet switching time, which could permit to propose an appropriate relation for the estimation of the oscillation frequency. This is not beyond the scope of this study and is therefore left for future works.

6. Conclusion

Two new configurations, based on interconnections between the feedback loops, have been proposed to synchronize two similar pulsed jet oscillators. These two configurations have been validated experimentally and numerically. The first one leads to a frequency close to the one of the oscillators working separately and the pulsed jets generated by these two devices are nearly in opposite phase. The second method leads to a much lower frequency and a phase difference close to a quarter oscillation period. It is also important to note that both synchronization configurations permit to eliminate the differences in the frequencies of the two oscillators working separately which were due to small geometrical deviations between the two devices. This phenomenon was confirmed numerically and demonstrates the robustness of the coupling *vis-à-vis* some limited geometrical deviations from one oscillator to the other.

Numerical simulations have also permitted to explain the dynamic behavior of the synchronized oscillators: pretty much like for individual oscillators, the oscillation mechanism is linked to the back and forth propagation of pressure waves in the oscillator's branches and feedback loops. In the first interconnection pattern, the frequency response is shown to be independent from the phase lag between the two oscillators. The simple relation established for a single oscillator to estimate its working frequency thus applies fairly well for the synchronized pair of actuators.

In the second interconnexion pattern, it has been shown that the jet switching time was no more negligible compared to the propagation time of the pressure waves along the feedback loops, leading to a lower oscillation frequency. In addition, the phase lag and the working frequency of the oscillator pair are closely linked. Additional experimental investigations are needed to better understand the physical mechanisms controlling the jet switching time, in order to propose a suitable relation for the estimation of the working frequency of the oscillators pair synchronized with the second interconnection pattern.

CRediT authorship contribution statement

Shiqi Wang: Conceptualization, Validation, Software, Writing - Original Draft**, Ahmad Batikh:** Supervision, Visualization, Writing - Review & Editing. **Lucien Baldas:** Methodology, Formal analysis, Supervision, Writing - Review & Editing**. Azeddine Kourta:** Methodology, Formal analysis, Supervision, Writing - Review & Editing**. Nicolas Mazellier:** Writing - Review & Editing**. Stéphane Colin:** Writing - Review & Editing**. Stéphane Orieux:** Investigation.

Declaration of Competing Interest

The authors declare that they have no known competing financial interests or personal relationships that could have appeared to influence the work reported in this paper.

Data availability

No data was used for the research described in the article.

Acknowledgement

This work was granted access to the HPC resources of CALMIP supercomputing center under the allocation 2018-P1507.

References

[1] G. Raman, A.B. Cain, Innovative actuators for active flow and noise control, Proc Inst Mech Eng G J Aerosp Eng (2002), https://doi.org/10.1243/095441002321029044.
[2] F. Sun, R.-S. Lin, M. Haas, T. Brogan, Air flow control by fluidic diverter for low NOx jet engine combustion, in: AIAA (Ed.), 1st Flow Control Conference, AIAA, St. Louis, Missouri, 2002: pp. 1–8.
[3] D. Guyot, B. Bobusch, C.O. Paschereit, S. Raghu, Active Combustion Control Using a Fluidic Oscillator for Asymmetric Fuel Flow Modulation, in: 44th AIAA/ASME/SAE/ASEE Joint Propulsion Conference & Exhibit, AIAA, Hartford, CT, 2008: pp. 1–19. https://doi.org/10.2514/6.2008–4956.
[4] S. Aubrun, J. McNally, F. Alvi, A. Kourta, Separation flow control on a generic ground vehicle using steady microjet arrays, Exp. Fluids 51 (2011) 1177–1187, https://doi.org/10.1007/s00348-011-1132-0.
[5] S.H. Kim, C. Kim, Separation control on NACA23012 using synthetic jet, Aerosp. Sci. Technol. 13 (2009), https://doi.org/10.1016/j.ast.2008.11.001.
[6] C. Lin, F. Hsiao, Experimental study of flow separation over NACA633018 wing with synthetic jet control at low Reynolds numbers, J. Mech. 29 (2013) 45–52, https://doi.org/10.1017/jmech.2012.120.
[7] A. Batikh, L. Baldas, S. Colin, Application of Active Flow Control on Aircrafts - State of the Art, in: International Workshop on Aircraft System Technologies, Hamburg, Germany, 2017: pp. 1–10.
[8] L. Löfdahl, M. Gad-el-Hak, MEMS applications in turbulence and flow control, Prog. Aerosp. Sci. 35 (1999), https://doi.org/10.1016/S0376-0421(98)00012-8.
[9] L.N. Cattafesta, M. Sheplak, L.N. Cattafesta III, M. Sheplak, L.N. Cattafesta, M. Sheplak, Actuators for active flow control, Annu. Rev. Fluid Mech. 43 (2011) 247–272, https://doi.org/10.1146/annurev-fluid-122109-160634.
[10] P. Tewes, L. Taubert, I. Wygnanski, On the use of sweeping jets to augment the lift of a λ-wing, 28th AIAA Applied Aerodynamics Conference (2010), https://doi.org/10.2514/6.2010-4689.
[11] D. Greenblatt, I.J. Wygnanski, The control of flow separation by periodic excitation, Prog. Aerosp. Sci. 36 (2000) 487–545.
[12] T. Berk, T. Medjnoun, B. Ganapathisubramani, Entrainment effects in periodic forcing of the flow over a backward-facing step, Phys. Rev. Fluids 2 (2017) 1–18, https://doi.org/10.1103/PhysRevFluids.2.074605.
[13] C. Cerretelli, E. Gharaibah, An Experimental and Numerical Investigation on Fluidic Oscillators For Flow Control, 37th AIAA Fluid Dynamics Conference and Exhibit. (2007) 1–9, https://doi.org/10.2514/6.2007-3854.
[14] J.W. Gregory, J.P. Sullivan, G. Raman, S. Raghu, Characterization of the microfluidic oscillator, AIAA J. 45 (2007) 568–576, https://doi.org/10.2514/1.26127.
[15] B.C. Bobusch, R. Woszidlo, J.M. Bergada, C.N. Nayeri, C.O. Paschereit, Experimental study of the internal flow structures inside a fluidic oscillator, Exp. Fluids 54 (2013), https://doi.org/10.1007/s00348-013-1559-6.
[16] V. Tesař, Taxonomic trees of fluidic oscillators, EPJ Web Conf. 143 (2017) 1–10, https://doi.org/10.1051/epjconf/201714302128.
[17] V. Tesař, S. Zhong, F. Rasheed, New fluidic-oscillator concept for flow-separation control, AIAA J. 51 (2013) 397–405, https://doi.org/10.2514/1.J051791.

[18] C. Cerretelli, K. Kirtley, Boundary layer separation control with fluidic oscillators, J. Turbomach. 131 (2009) 041001, https://doi.org/10.1115/1.3066242.
[19] J.W. Gregory, M.N. Tomac, A Review of Fluidic Oscillator Development and Application for Flow Control, in: AIAA (Ed.), 43rd Fluid Dynamics Conference, San Diego, CA, 2013: pp. 1–26. https://doi.org/10.2514/6.2013–2474.
[20] R. Woszidlo, F. Ostermann, H.J. Schmidt, Fundamental properties of fluidic oscillators for flow control applications, AIAA J. 57 (2019), https://doi.org/10.2514/1.J056775.
[21] J. KIRSHNER, S. KATZ, Design Theory of Fluidic Components., 1975. https://doi.org/10.1016/b978–0-12–410250-7.x5001–7.
[22] J.R. Tippetts, H.K. Ng, J.K. Royle, A fluidic flowmeter, Automatica 9 (1973) 35–45, https://doi.org/10.1016/0005-1098(73)90010-1.
[23] X. Meng, C. Xu, H. Yu, Feedback fluidic flowmeters with curved attachment walls, Flow. Meas. Instrum. 30 (2013) 154–159, https://doi.org/10.1016/j.flowmeasinst.2013.02.006.
[24] B.C. Bobusch, R. Woszildo, O. Kruger, C.O. Paschereit, Numerical Investigations on Geometric Parameters Affecting the Oscillation Properties of a Fluidic Oscillator, AiAA 2013–2709. (2013) 1–15. https://doi.org/10.2514/6.2013–2709.
[25] R. Seele, P. Tewes, R. Woszidlo, M.A. McVeigh, N.J. Lucas, I.J. Wygnanski, Discrete sweeping jets as tools for improving the performance of the V-22, J. Aircr. 46 (2009) 2098–2106, https://doi.org/10.2514/1.43663.
[26] R. Woszidlo, I. Wygnanski, Parameters governing separation control with sweeping jet actuators, 29th AIAA Appl. Aerodyn. Conf. 19 (2011), https://doi.org/10.2514/6.2011-3172.
[27] R. Woszidlo, F. Ostermann, C.N. Nayeri, C.O. Paschereit, The time-resolved natural flow field of a fluidic oscillator, Exp. Fluids 56 (2015) 1–12, https://doi.org/10.1007/s00348-015-1993-8.
[28] A. Jafarian Amiri, M. Farhadi, Numerical investigation of a single feedback loop oscillator with two outlet channels, Chem. Eng. Res. Des. 150 (2019), https://doi.org/10.1016/j.cherd.2019.07.031.
[29] G. Arwatz, I. Fono, A. Seifert, Suction and Oscillatory Blowing Actuator Modeling and Validation 46 (2008), https://doi.org/10.2514/1.30468.
[30] S. Gokoglu, M. Kuczmarski, D. Culley, S. Raghu, Numerical Studies of an Array of Fluidic Diverter Actuators for Flow Control, in: 41st AIAA Fluid Dynamics Conference and Exhibit, American Institute of Aeronautics and Astronautics, Reston, Virigina, 2011: pp. 27–30. https://doi.org/10.2514/6.2011–3100.
[31] M. Shigeta, T. Miura, S. Izawa, Y. Fukunishi, Active control of cavity noise by fluidic oscillators, Theor. Appl. Mech. Jpn. 57 (2009) 127–134, https://doi.org/10.11345/nctam.57.127.
[32] S. Aram, H. Shan, Synchronization effect of an array of sweeping jets on a separated flow over a wall-mounted hump, in: AIAA Aviation 2019 Forum, American Institute of Aeronautics and Astronautics Inc, AIAA, 2019: pp. 1–16. https://doi.org/10.2514/6.2019–3396.
[33] F. Ostermann, R. Woszidlo, C.N. Nayeri, C.O. Paschereit, The interaction between a spatially oscillating jet emitted by a fluidic oscillator and a cross-flow, J. Fluid Mech. 863 (2019), https://doi.org/10.1017/jfm.2018.981.
[34] M.A. Hossain, R. Prenter, R.K. Lundgreen, L. Agricola, A. Ameri, J.W. Gregory, J. P. Bons, Investigation of Crossflow Interaction of an Oscillating Jet, 55th AIAA Aerospace Sciences Meeting (2017) 1–11, https://doi.org/10.2514/6.2017-1690.
[35] C. Cerretelli, K.R. Kirtley, Method and system for flow control with fluidic oscillators, US7128082B1, 2006.
[36] M. Koklu, Fluidic oscillator array for synchronized oscillating jet generation, US9333517B2, 2016.
[37] M.N. Tomac, J.W. Gregory, Phase-synchronized fluidic oscillator pair, 47th AIAA Fluid Dynamics Conference (2017) 1–15, https://doi.org/10.2514/6.2017-3314.
[38] M. Tomac, J. Gregory, Frequency-Synchronized Fluidic Oscillator Array, US11085469B2, 2018.
[39] E. Sundström, M.N. Tomac, Aeroacoustic characteristics of a synchronized fluidic oscillator, Flow. Turbul. Combust. 106 (2021) 61–77, https://doi.org/10.1007/s10494-020-00193-3.
[40] E.T. Sundström, M.N. Tomac, Synchronization and flow characteristics of the opposed facing oscillator pair in back-to-back configuration, Flow. Turbul. Combust. 104 (2020) 71–87, https://doi.org/10.1007/s10494-019-00064-6.
[41] M.N. Tomac, M.A. Hossain, Flow and frequency characterization of the synchronized stacked sweeping jets, AIAA J. 59 (2021), https://doi.org/10.2514/1.J059643.
[42] M.N. Tomac, Novel jet impingement atomization by synchronizing the sweeping motion of the fluidic oscillators, J. Vis. (Tokyo) 23 (2020), https://doi.org/10.1007/s12650-020-00632-3.
[43] A. Seifert, I. Dayan, T. Shtendel, Synchronization of fluidic actuators, WO 2013/061276 Al, 2013.
[44] M. Bauer, J. Lohse, F. Haucke, W. Nitsche, High-lift performance investigation of a two-element configuration with a two-stage actuator system, AIAA J. 52 (2014) 1307–1313. ⟨http://arc.aiaa.org/doi/abs/10.2514/1.J052639⟩.
[45] S. Wang, L. Baldas, S. Colin, S. Orieux, A. Kourta, N. Mazellier, I. Introduction, Experimental and numerical study of the frequency response of a fluidic oscillator for active flow control, in: 8th AIAA Flow Control Conference AIAA, AIAA Aviation, Washington, D.C., 2016: pp. 1–15. https://doi.org/10.2514/6.2016–4234.
[46] S. Wang, A. Batikh, L. Baldas, A. Kourta, N. Mazellier, S. Colin, S. Orieux, On the modelling of the switching mechanisms of a Coanda fluidic oscillator, Sens Actuators A Phys. 299 (2019) 1–12, https://doi.org/10.1016/j.sna.2019.111618.
[47] R. Khelfaoui, S. Colin, S. Orieux, R. Caen, L. Baldas, Numerical and experimental analysis of monostable mini- and micro-oscillators, Heat. Transf. Eng. 30 (2009) 121–129, https://doi.org/10.1080/01457630802293548.
[48] H. Coanda, Device for deflecting a stream of elastic fluid projected into an elastic fluid, US Patent 2,052,869. (1936) 1935–1937.
[49] L. Zhou, S. Wang, J. Song, Z. Li, X. Liu, D. Peng, X. Wen, Y. Liu, Study of internal time-resolved flow dynamics of a subsonic fluidic oscillator using fast pressure sensitive paint, Exp. Fluids (2022) 1–16, https://doi.org/10.1007/s00348-021-03370-w.

Shiqi Wang is an engineer in 'Aero-Engine Academy of China'. He received his Ph.D. in fluid dynamics in 2017 from the University of Toulouse. He is currently working on the development of actuators for active flow control, especially the fluidic oscillator actuation system. He is also working on flow control technology application in gas turbine engines.

Ahmad Batikh is an Associate Professor of energy engineering at 'Institut Catholique des Arts et Métiers' (Icam) of Toulouse, and associate researcher at the Institut Clément Ader (ICA) in Toulouse, France. In 1998, he graduated from the Aleppo University (Syria), and he received his Ph.D. in mechanical engineering in 2008 from INSA of Toulouse. His current research focuses on fluidic actuators for flow control and heat transfer enhancement and on the development of innovative heat sinks for cooling power electronics.

Lucien Baldas is an Associate Professor of mechanical engineering at the National Institute of Applied Sciences (INSA) of Toulouse, France. He received his Ph.D. in fluid mechanics in 1993 from the National Polytechnic Institute of Toulouse. His current research, at the Institut Clément Ader in Toulouse, focuses on compressible flows in pneumatic systems and on microfluidics with a special interest in rarefied gaseous flows in microsystems and in micro fluidic actuators for flow control and heat transfer enhancement. He is currently the head of Microfluidics team at the ICA.

Azeddine Kourta is a Professor at the Polytechnique Engineer School of the University of Orléans since September 2008. Since 1988, he was a Senior Researcher at CNRS and the Head of the EMT2 Group "Ecoulements Monophasiques Transitionnels et Turbulents" (One phase transitional and turbulent flows) at IMFT (Institut de Mécanique des Fluides de Toulouse). He is the head of PRISME laboratory (Pluridisciplinaire de Recherche en Ingénierie des Systèmes, Mécanique, Energétique). He is the Vice-Director of GDR 2502 of CNRS the French network on "Flow Separation Control". Their area of expertise are active flow control, transition and turbulence, unsteady and compressible flows, aerodynamics and aeroacoustics.

Nicolas Mazellier is a Professor at the University of Orléans, France. In 2002, he graduated from the Polytechnic National Institute of Grenoble (France). He received his PhD in Fluid Mechanics from the University Joseph Fourier (France) in 2005. He obtained a postdoctoral fellowship at Department of Aeronautics in Imperial College London (UK) from 2006 to 2007 and then at the University of Rouen (France) from 2007 to 2009. His current research activities are dedicated to turbulent separated flows encompassing separating/reattaching flows and wakes with a particular interest in the modelling of transfer mechanisms at interfaces.

Stéphane Colin is a Professor at the University of Toulouse, France, since 2002. He obtained an Engineer degree in 1987 and received his PhD in Fluid Mechanics from the Polytechnic National Institute of Toulouse in 1992. He created in 1999 the Microfluidics Group of the Hydrotechnic Society of France and launched the series of Microfluidics European Conferences. His current research is mainly focused on gas microflows, with a particular interest in the experimental analysis of rarefied flows. He is currently the head of the Modeling and Simulation of Systems and Microsystems Group of Institut Clément Ader (ICA) in Toulouse, and Associate Editor of *Microfluidics and Nanofluidics*.

Stéphane Orieux is a research engineer at the Institut Clément Ader (ICA) in Toulouse, France. He received his Ph.D. in 1999 from the National Institute of Applied Sciences (INSA) of Toulouse. He is a specialist in modelling and design and experimental analysis of pneumatic and electromechanical systems and microsystems.